

ANALYTICAL AND EXPERIMENTAL DATA OF CHEST DEFLECTIONS AND INJURIES IN SIDE IMPACTS

Narayan Yoganandan, Frank A. Pintar, John R. Humm, Jason J. Hallman, Dennis J. Maiman

Medical College of Wisconsin

Milwaukee, WI USA

Paper number 11-0256

ABSTRACT

Studies using post mortem human subjects (PMHS) are conducted for the design and evaluation of dummies. Biomechanical variables such as forces, accelerations, and deflections are used to characterize responses under simulated environments including frontal, rear, nearside and far-side impacts. The present paper is focused on the nearside occupant. Chest and abdominal deflections are important variables in this mode because real-world injuries to these regions of the human body are shown to correlate with occupant kinematics during the loading event. Consequently, this paper focuses on kinematic data from PMHS tests. Specifically, deflections obtained from chestbands placed on the outer periphery of the thorax and abdomen, and injury data from simulated pure lateral, anterior oblique, and posterior oblique impacts are presented.

INTRODUCTION

Sled tests are often conducted to compare responses of different surrogates (PMHS and dummies) under predetermined initial and boundary conditions in a laboratory environment. Such tests are essential during dummy design and development as it is critical to mimic the human response during impact [1-6]. In crashworthiness research, PMHS responses are commonly used as a benchmark [7-10]. This process, in vogue for more than half a century, has been a major tool for regulators around the world, component suppliers, and other agencies such as the Insurance Institute for Highway Safety in the evaluation of the safety of motor vehicles [11-13]. The present paper focuses on side impacts.

Side impact-induced injuries have been categorized based on the direction of the impact force. From a historical perspective, pure lateral, that is, clock positions of nine for the driver and three for the passenger in the United States, are commonly used as the direction of the loading vector for the evaluation of biomechanics and motor vehicle crashworthiness [10, 14-17]. Analyses using the United States National Automotive Sampling System (NASS-CDS) and Crash Injury Research and Engineering Network

(CIREN) have identified anterior-directed oblique, in addition to pure lateral, as another vector associated with trauma to the chest, abdomen, and pelvis in real world side impacts [18]. Because the impact vector is oblique, deflection patterns imparted to the human torso differ from those induced by the pure lateral vector. Recognition of this vector and quantification of biomechanical data requires tests with PMHS in simulated sled environments. These tests produce peak deflections in the anterior oblique directions due to orientation of the impact.

Recent epidemiological and case-specific analyses from NASS and CIREN databases have shown the importance of posterior-directed oblique loading of the thorax in lateral impacts in modern motor vehicle environments. In 2010, Hallman et al. advanced a theory wherein side airbags deployed during impact, may act as a source for spleen and kidney traumas [19]. Mathematical models incorporating side airbag in the simulation of occupant kinematics have delineated the role of posterior-directed thoracic and abdominal deflection in the injury process [20]. In order to better understand the role of this loading vector on injury biomechanics, tests are necessary with PMHS in simulated sled environments.

Consequently, the aim of this paper is to provide side impact data from PMHS sled tests conducted under the above discussed load vectors. Chest and abdomen deflections and injury-related data are given under pure lateral, anterior oblique, and posterior oblique impacts.

METHODS

Pure Lateral Impacts

Specimen Preparation: Unembalmed PMHS were procured, medical records evaluated, and screened for HIV, and Hepatitis A, B, and C before specimen preparation for sled tests. Anthropomorphic data and pretest x-rays were obtained according to established procedures [17]. All specimens were dressed in tight-fitting leotards, and a mask covered the head/face. Prepared subjects were placed on a Teflon-coated bench seat fixed to the platform of a

deceleration sled, configured with an impacting load wall to simulate side impact. The bench seat was 1.3 m long. Four plates (upper plate for measuring contact forces with the mid-thorax, middle plate for the abdomen, lower plate for the pelvis, and extremity plate for the lower extremities) were used in the load wall design. Figure 1 shows the schematic of the load wall and buck.

The configuration of the load wall was such that specimens impacted the wall with the force vector perpendicular to the path of travel of the specimen or with no anterior or posterior obliquity, i.e., pure lateral impact. While the mode was pure lateral, the wall had a flat, pelvic or thoracic offset achieved by moving the lower or upper plate closer to the specimen. The offset was set at 100 mm. The vertical height of the upper edge of the thoracic plate was set at 400 mm to prevent shoulder contact. Figure 2 shows a schematic of the specimen and the targeted impact locations along with the load wall, based on mid-size male anthropometry. Tests were done at 6.7 and 8.9 m/s (low and high) velocities.

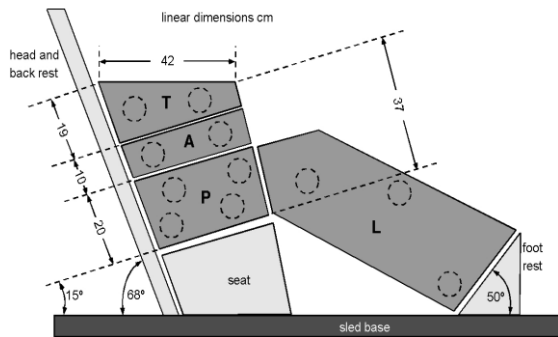


Figure 1: Schematic of the buck showing the load plates (T: thorax, A: abdomen, P: pelvis, and L: lower leg).

Initial Positioning

The initial positioning was such that the Frankfort plane was horizontal, legs were stretched parallel to the mid-sagittal plane, and curvature and alignment of the dorsal spinal column were maintained without any pre-torso rotation in the axial plane. The right-handed Cartesian coordinate system of reference was followed according to the Society of Automotive Engineers (SAE) specifications, i.e., the positive x-acceleration was along the posterior-anterior direction, positive y-axis acceleration was along the left-right axis, and positive z-axis acceleration was along the superior-inferior direction.

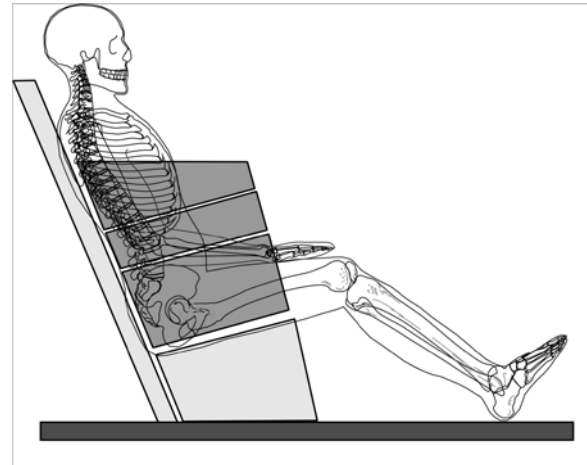


Figure 2: Schematic of targeted impact locations from the four plates onto the specimen, assuming mid-size anthropometry.

The specimen contacted the initially configured flat load wall (padded or rigid) without changes in the anatomical interrelationships between the various body segments. The entire pelvis up to the level of the iliac crest contacted the pelvic load plate. The abdominal load plate was exposed to lower regions of the ribcage while the thoracic load plate engaged the section of the middle ribcage. Tests included rigid and padded impacts. The padding was 10-cm thick, LC200 type. The compressive stiffness was 103 kPa.

Instrumentation

A uniaxial accelerometer was used on the sled to record the input velocity; and tri-axial accelerometers were fixed to the upper thoracic spine (T1), lower thoracic spine (T12), and sacrum (Figure 3). To record medial-lateral accelerations of the struck-side ribcage, uni-axial accelerometers were fixed to the left side of ribs four and eight and sternum. Eleven load cells (two each in the thorax and abdomen, four in the pelvis, and three in the extremity) were used to record the dynamic forces. Chestbands were fixed at the axilla (upper), xyphoid process (middle), and tenth rib (lower) to measure deformation-time histories. Chestband signals were filtered at class 600, and deformation contours were computed at 250 one-millisecond intervals. Starting at the spine and following the contour clockwise path, locations were identified at 20, 25, and 30% of the circumference (Figure 4). A line was drawn between the sternum (one-half of contour circumferences) and spine on each contour, and the three identified locations were projected onto the sternum-spine line. The distance

was measured between each point on the contour of the left side of the thorax and the projected sternum-spine line. The resulting three measurements (0, 25 and 30 percent circumference) were averaged to obtain the mean deflection. The process was repeated at all time intervals to obtain left-half chest deflection-time plot. Normalized chest deflections were obtained by dividing this deflection by the one-half depth of the PMHS chest.

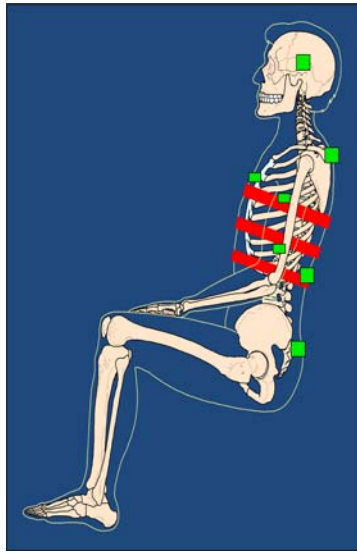


Figure 3: Instrumentation showing chestbands and accelerometers on the spine and head.

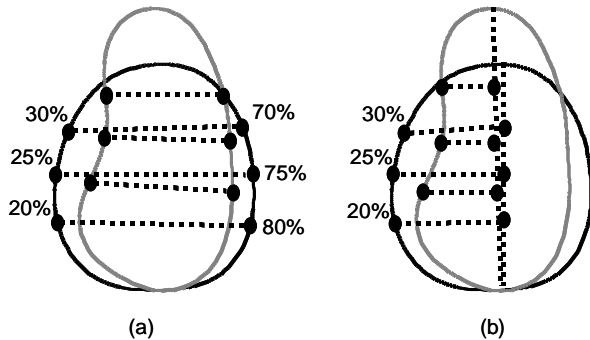


Figure 4: Schematic to determine full (a) and half (b) deflections from chestband contours.

Following the test, specimens were palpated, a clinical-type examination for stability was performed by the clinical personnel, x-rays were obtained, an autopsy was conducted, and traumas were graded based on the Abbreviated Injury Scale [21].

Anterior Oblique Impacts

The experimental protocol used for anterior oblique impacts were based on pure lateral impacts. The setup was configured, as before, for left side impacts. The specimens were seated upright with the Frankfort plane horizontal, legs stretched parallel to the mid-sagittal plane, and normal curvature and alignment of the dorsal spine was maintained without any initial torso rotation. Frontal and overhead schematic views of the test setup are shown in figures 5 and 6. To simulate an oblique lateral impact, the abdominal and thoracic plates of the wall were angled 20- or 30-degrees.

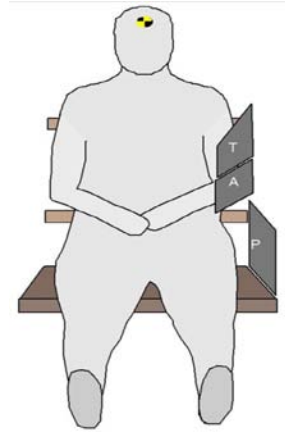


Figure 5: Frontal view showing the positioning for anterior oblique impact tests. The same four load wall plates used in pure lateral impacts were used in this series. Figure 1 shows plate details and dimensions, and figure 6 shows the overhead view of the setup.

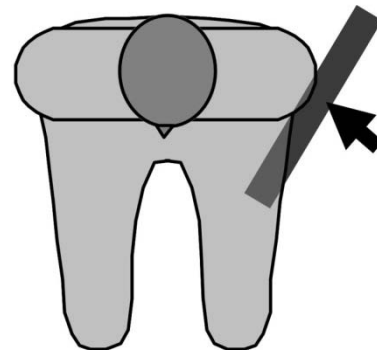


Figure 6: Overhead view showing positioning for anterior oblique impact tests. The arrow indicates the direction of the impacting load vector. Figure 5 shows the frontal view, albeit to a different scale.

Contours of chest deflections at the three thoracic levels were computed at every millisecond. Using palpation, the spine location corresponding to PMHS spinous process was identified and two closest gages bilateral to the anatomy were located. The center of the line joining the two gages defined the origin and the “spine” on the contour. The sternum location on the contour was identified as the point diametrically opposite to the “spine”. These sternum and spine locations defined the reference line for determining one-half chest deflections on the struck side. After defining the spine and sternum locations on the undeformed contour, or on the contours before time-zero, these locations were used to define half deflection values throughout the event. On the undeformed contour, the midpoint of the line segment joining the spine and sternum was located and the distance from the spine point to midpoint was recorded. This distance was used to continue to define the reference point from which the half deflection measures were obtained throughout the deforming contour time history. Temporal deflection at any specific location on the chest was defined as the change in the distance between the line joining the location and the reference point in the initial undeformed chest contour and the deformed contour at any instant. Peak deflection was determined from these time histories (Figure 7).

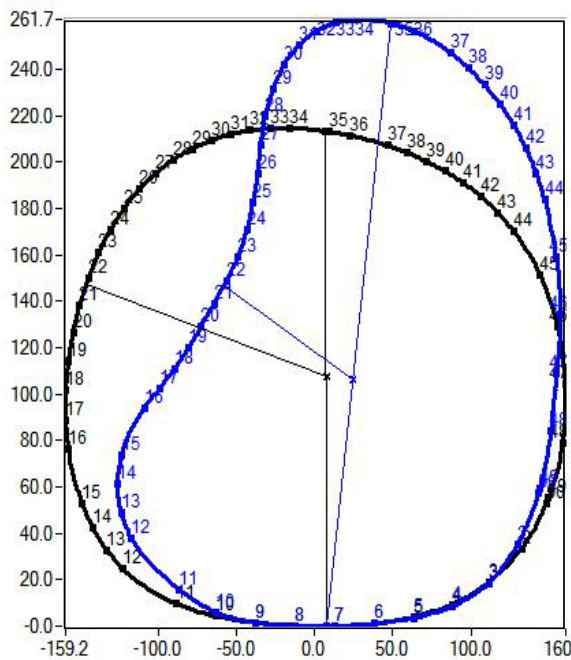


Figure 7: Contours showing the method used to define maximum deflections from the chestband.

Posterior Oblique Impacts

Although the loading patterns for posterior oblique impacts were different, as in the case of the previous load vectors, specimens were seated upright with the Frankfort plane horizontal, legs stretched parallel to the mid-sagittal plane, and the normal curvature and alignment of the dorsal spine maintained without any initial torso rotation. Loading was induced by attaching a side airbag to the load wall, shown in figure 8 [19]. Static and dynamic deployments tests were conducted. In the former, the airbag was deployed to the stationary PMHS, and in the latter, the airbag was deployed using the sled load wall with the PMHS moving towards the wall, similar to the previous two vectors. In static tests, the airbag was mounted approximately 130 mm away from the wall, subjects were positioned approximately 100 mm from the T6-L1 posterolateral thorax to contact the airbag, and sequential bilateral deployment tests were conducted. In dynamic tests, the airbag was mounted approximately 150 mm away from the wall, subjects were positioned 400 mm from the wall, and the airbag was activated when the outboard edges of the module and torso were coincident in the frontal plane to ensure airbag interaction with the posterolateral region of the thorax and abdomen. In static tests, one 59-channel chestband was placed at the xyphoid level, and in dynamic tests, two chestbands were used at the xyphoid and tenth rib levels.

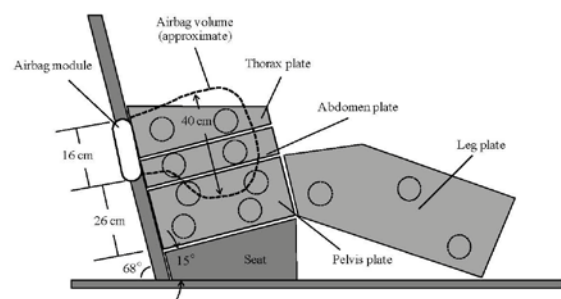


Figure 8: Schematic of the buck showing the four plates (see figure 1 for details) and the side airbag used in static and dynamics tests for posterior oblique loading.

Chestband contours were processed by shifting the contour-based spine and sternum to the right side (10% of circumference) of the subject-specific spine and sternum. The origin was defined as the midpoint between the spine and sternum contour locations at

time zero. As deformation progressed, the origin remained coincident with the spine-sternum axis and maintained a fixed distance from the spine. Net deflections at discrete locations were quantified, normalized to the initial chest breadth, and processed using CFC 180 filter (Figure 9). Similar to the earlier modes of loading, injuries were identified using x-rays and autopsy, and were graded based on the Abbreviated Injury Scale [21].

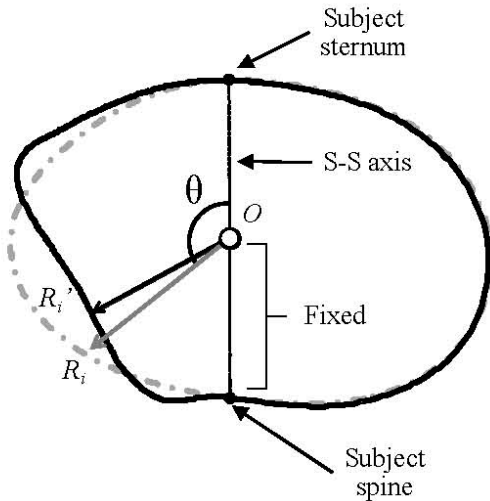


Figure 9: Schematic of the chestband contour for left side posterior oblique loading. S-S refers to the spine-sternum axis. The difference between the two vectors represents the chest deflection.

RESULTS

Figure 10 shows a typical, square wave shape sled pulse used in all tests. Deflection data are described followed by injury results.

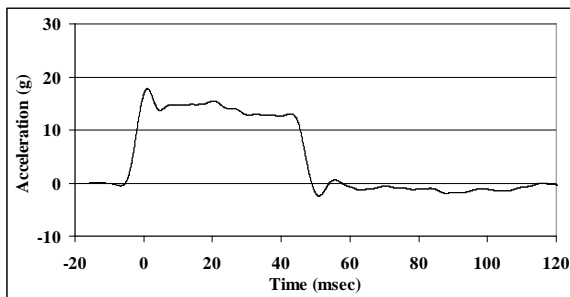


Figure 10: Typical sled pulse.

Pure lateral Impacts

Anthropometric data from 26 PMHS were such that the average age was 62 years, stature was 173 cm, and body mass was 71 kg. Deflection-time signals were unimodal. Corridor data are given [16]. Table 1 summarizes peak deflections of the upper thorax, lower thorax, and abdomen as a function of initial conditions. The upper and lower thoracic deflections were not significantly influenced by the change in test conditions. The time of maximum upper thorax deflection was dependent upon test condition and peaked earliest in the rigid high-speed condition, followed by the padded high-speed, rigid low-speed, and padded low-speed. Similar trends occurred in the lower thoracic deflection; however, discrimination between time of peak was not as pronounced since the rigid low-speed and padded high-speed test results overlapped. Abdominal deflections in the high-speed condition were greater than those in the low-speed condition. The reader is referred to the original paper for deflection-time histories under each condition.

Table 1: Summary of peak deflections from pure lateral impacts. R and P refer to rigid and padded, H and L refer to high and low speed, and F refers to flat wall, respectively.

Test Condition		Deflection (mm)			
		RHF	PHF	RLF	PLF
Measurement Location					
Upper thorax	Full	95	89	110	85
	Half	58	60	72	56
	Half/Full	61%	67%	66%	66%
Lower thorax	Full	93	100	82	82
	Half	58	55	51	52
	Half/Full	62.40%	55.00%	62.20%	63.40%
Abdomen	Full	n/a	118	86	98
	Half	n/a	78	52	58
	% Half/Full	n/a	66.10%	60.50%	59.20%

While the upper and lower thoracic deflections were not considerably influenced by test conditions, their times of occurrence depended on test condition and peaked earliest in the rigid high-speed condition, followed by the padded high-speed, rigid low-speed, and padded low-speed. Abdominal deflections were greater in the high-speed than the low-speed test condition.

Anterior Oblique Impacts

Anthropometric data from four specimens were such that the mean age, stature, and total body mass were 55 years, 173 cm, and 59 kg. Peak deflections at the upper, middle, and lower levels of the chest, from the

three temporal chestband contours, on a test-by-test basis, are given in table 2. The mean maximum deflections at the upper, middle and lower levels of the chest for the 30-degree tests were 96.2, 78.5, and 76.8 mm, and for the 20-degree tests, the peak deflection magnitudes were 77.5, 89.9, and 73.6 mm, respectively.

A comparison of deflections from pure lateral and anterior oblique loadings is shown in figure 11. Peak deflections at the upper level were similar between the two groups of tests; at the mid and lower levels, peak deflections were greater in both oblique loadings compared to pure lateral tests, indicating the effect of the obliqueness of the load vector. Although the magnitudes of deflections are the same for the upper band, if deflections are at different locations, the injury tolerance might be less at that thoracic region. While peak deflections at the upper chest level were not different between oblique and pure lateral tests ($p > 0.05$), at the mid and lower thoracic levels peak deflections were significantly greater ($p < 0.05$) in oblique than pure lateral tests.

Table 2: Summary of specimen-specific peak deflections (mm) from anterior-oblique impacts from four specimens.

Test Description	Upper	Middle	Lower
20-degree PMHS test 1	69.6	69.4	69.5
20-degree PMHS test 2	85.3	110.4	77.6
30-degree PMHS test 1	90.5	75.1	86.3
30-degree PMHS test 2	101.9	81.9	67.3

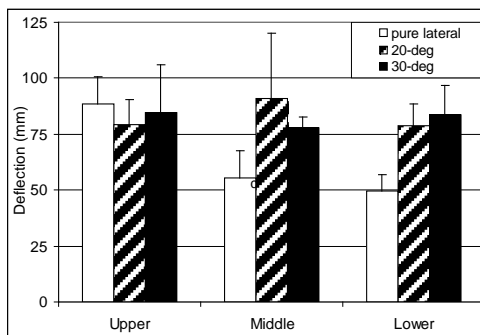


Figure 11: Comparison of the peak deflections at the three thoracic levels between pure lateral and anterior oblique impact tests. Error bars indicate standard deviations.

Posterior Oblique Impacts

Anthropometric data of seven PMHS (three static and four dynamic tests) were such that the mean age, stature, and total body mass were 61 years, 170 cm, and 92 kg. Deformations ensued from the posterior-lateral region of the thorax and abdomen due to airbag interaction in both tests. Table 3 shows a summary of peak deflections along with the angle and time of occurrence on a specimen-by-specimen basis. Maximum deflections occurred between 100 and 110 deg in dynamic and 115 and 135 deg in static tests. A comparison of the mean deflection angles from pure lateral, and anterior and posterior oblique loadings is shown (Figure 12). Deflection angles were in-line with the impact vector in the former two types of tests. At the onset of deflection, mean deflection angle was significantly greater (t-test; $p < 0.001$; 35 deg) in dynamic than pure lateral and anterior oblique tests. Further, both posterior oblique tests showed transient deflection loci ranging from 20 to 30 deg during the first 60 ms of impact; deflection angles resulting from pure lateral and anterior oblique impacts did not vary by more than five deg. Further details along with deflection corridors are given [19].

Table 3: Peak chest deflections at different levels in static (S) and dynamic (D) tests.

PMHS	Location	Peak	Time	Angle
		mm	(ms)	(deg)
S-1	Xyphoid	39.84	14.6	135
S-2	Xyphoid	29.56	21.4	99
S-3	Xyphoid	58.26	22.0	132
S-4	Xyphoid	41.88	12.8	128
S-5	Xyphoid	23.88	23.2	116
S-6	Xyphoid	53.27	16.9	128
D-1	Axilla	69.58	31.2	112
	Xyphoid	64.36	27.3	103
D-2	Xyphoid	113.52	26.7	99
	Rib 10	74.34	36.0	102
D-3	Xyphoid	56.36	18.1	110
	Rib 10	41.32	33.4	98
D-4	Xyphoid	52.10	21.5	108
	Rib 10	66.42	25.4	125

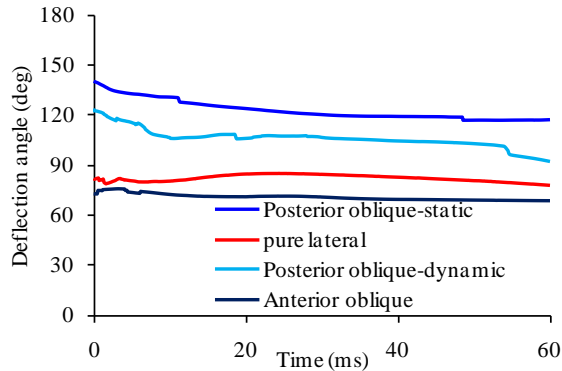


Figure 12: Comparison of the peak deflections between pure lateral, and anterior and posterior oblique impact tests.

Injuries

In general, skeletal injuries in the form of rib fractures were most prevalent in pure lateral and anterior oblique loadings. In pure lateral impact loading, skeletal traumas ranged from AIS 0 to 4 [21]. However, at the high velocity loading of 8.9 m/s, internal organ trauma occurred.

Anterior oblique impacts also showed similar skeletal injury predominance: in the 30- and 20-degree series, one specimen sustained AIS 3 and the other sustained AIS 4 trauma. In both specimens with AIS 3 trauma, unilateral fractures and single fracture to any specific rib were identified. Thirty-degree tests produced fractures to the ribcage including fracture to the first rib; and in the 20 deg tests, while inducing rib fractures, the first rib was not involved, and soft tissue injuries were identified as lung contusions and diaphragm laceration along with a flail chest in the specimen that sustained the greatest injury severity. The pleural tear attributed to the fracture of the seventh rib occurred at its lateral end. In contrast, the diaphragm laceration was not in the vicinity of the rib fracture. Traumas were not produced to renal or spleen structures.

In contrast, in posterior oblique impacts under static testing, out of the three specimens, one had no injury, another had AIS 3 level rib fractures, and the third specimen sustained AIS 3 skeletal and AIS 2 spleen laceration. In dynamic tests, all specimens sustained skeletal or visceral injuries: three sustained rib fractures (AIS 3 in two and 4 in one); and three sustained visceral (renal and spleen laceration; AIS 2 in two specimens), and left inferior labrum (AIS 3) lacerations.

DISCUSSION

Differences were found in the pattern regarding the peak and attainment of peak deflections between the three modes of impacts. This finding may assist in evaluating side impact dummies, from deflection-related metrics, an approach used in pure lateral impact biofidelity evaluations [22].

An anterior oblique impact, of the same severity and to the same level of the chest as the pure lateral impact, engages the same internal organ differently. At the upper thoracic region, the pure lateral vector directly loads regions dorsal to the subclavian artery while an oblique vector at 30 deg applies forces to the ventral arterial regions engaging the common carotid artery and brachio-cephalic vein. The former force vector introduces posteroanterior load transfer, in contrast to antero-posterior load transfer by the oblique vector. The ribcage is loaded in direct compression at its most lateral region under pure lateral loading in contrast to the angulated compression at the antero-lateral region by the oblique vector. The anterior regions of the thoracic vertebral body sustains lateral shear in the pure loading case. It resists antero-lateral shear in the oblique case. Spine is weaker antero-posteriorly. At an inferior level, while the aorta is protected by the stomach in the pure lateral loading, in the oblique case, the major vessel is protected by the relatively smaller liver lobe and its articulations [23].

Similar regional load transfer mechanisms are apparent as the impact vector traverses caudally. Pure anatomical considerations with respect to the impact vector, in addition to the functional and constitutive differences, may contribute to the mechanism of load transfer and injury. Deflections being a hallmark for these injuries, it is important to delineate this metric. Results in this paper serve as a first step in the process.

While deflection angles remained essentially aligned with the impact vector over the entire loading event in pure lateral and anterior oblique cases, data were different in the posterior oblique loading. This is due to the interaction of the PMHS with the airbag. The area of contact from the deploying airbag with the PMHS torso is more transient than in the rigid wall case regardless of the impacting vector. From this perspective, the deflection magnitude and the time of occurrence may have been influenced by the chosen airbag system. Parametric studies may be needed to examine the role of variables such as the volume, venting pattern, and pressure on the deflection variable. Mean peak deflections occurring at 130 and

108 deg for the static and dynamic posterior oblique loading cases may have also been influenced by the type of the airbag system used in the present study.

Regarding the potential role of these posterior-lateral directed deflections due to airbag interaction on injuries, an analogy similar to the anterior oblique loading can be applied. The posterior oblique vector induces focal loading to the local upper abdominal organs such as spleen. Rib fractures correlated to peak local deflection may also be an outcome, as documented in literature [19]. The role of deflection and its associated secondary variables, such as rate of deflection and viscous criterion, may be important in the analyses of real-world internal injuries.

Regarding injuries and their potential mechanisms, skeletal trauma has been associated with deflections while internal organ trauma is associated with metrics such as rate of compression [10]. The relatively infrequent or absence of visceral trauma in pure lateral and anterior oblique tests, and the more commonly observed spleen and renal traumas in the posterior oblique impacts, may suggest that skeletal trauma is a direct consequence of impact loading to the rib cage while internal organ injury may be modulated by the initial absorption and transmission of the energy by the skeletal structure. From this perspective, internal organ injuries may be more complex, and need further research.

In summary, the present paper provides information on deflections and injuries in side impacts under pure lateral, anterior and posterior oblique vectors. These data are valuable to assess the biofidelity of anthropomorphic test devices such as the ES-2re and WorldSID, and assist in improving occupant safety in these environments.

ACKNOWLEDGMENTS

This study was supported in part by DTNH22-07-H-00173, and VA Medical Research. The assistance of Neuroscience research staff is acknowledged.

REFERENCES

1. Backaitis, S.H. and H.J. Mertz, eds. *Hybrid III: The First Human-Like Crash Test Dummy*. 1994, Society of Automotive Engineers: Warrendale, PA. 830.
2. Backaitis, S.H. and D.C. Viano, *Side Impact: Injury Causation & Occupant Protection*, ed. I.I.C.a. Exposition. Vol. SP769. 1989. 191 pp.
3. Yoganandan, N., F. Pintar, and T. Gennarelli. *Evaluation of side impact injuries in vehicles equipped with side airbags*. in *IRCOBI*. 2005. Prague, Czech Republic.
4. Yoganandan, N., F. Pintar, T. Gennarelli, and M. Maltese. *Patterns of abdominal injuries in frontal and side impact*. in *AAAM*. 2000. Chicago, IL.
5. Yoganandan, N. and F.A. Pintar, *Biomechanics of human thoracic ribs*. *J Biomech Engr*, 1998. **120**: p. 100-104.
6. Yoganandan, N. and F.A. Pintar, *Acceleration, deflection, and force corridors for small females in side impacts*. *Traf Inj Prevention*, 2005. **6**: p. 1-8.
7. Tarriere, C., G. Walfisch, A. Fayon, C. Got, and F. Guillon. *Synthesis of human impact tolerance obtained from lateral impact simulations*. in *7th Int'l Tech Conf on Experimental Safety Vehicles*. 1979. Washington, DC.
8. Viano, D., I. Lau, C. Asbury, A. King, and P. Begeman, *Biomechanics of the human chest, abdomen, and pelvis in lateral impact*. *Accid Anal & Prev*, 1989. **21**(6): p. 553-574.
9. Viano, D.C., I.V. Lau, D.V. Andrzejak, and C. Asbury, *Biomechanics of injury in lateral impacts*. *Accid Anal Prev*, 1989. **21**(6): p. 535-51.
10. Yoganandan, N., F.A. Pintar, B.D. Stemper, T.A. Gennarelli, and J.A. Weigelt, *Biomechanics of side impact: injury criteria, aging occupants, and airbag technology*. *J Biomech*, 2007. **40**(2): p. 227-43.
11. Yoganandan, N., R.M. Morgan, R.H. Eppinger, F.A. Pintar, A. Sances, Jr, et al., *Mechanism of thoracic injury in a frontal impact*. *J Biomech Engr*, 1996. **118**: p. 595-597.
12. Yoganandan, N., R.M. Morgan, R.H. Eppinger, F.A. Pintar, D.A. Skrade, et al., *Thoracic deformation and velocity analysis in frontal impact*. *J Biomech Engr*, 1995. **117**: p. 48-52.
13. Yoganandan, N., F. Pintar, and T. Gennarelli, *Field data on head injuries in side airbag vehicles in lateral impact*. *AAAM*, 2005. **49**: p. 171-184.
14. Cavanaugh, J.M., Y. Zhu, Y. Huang, and A.I. King, *Injury and response of the thorax in side impact cadaveric tests*, in *Biomechanics of Impact Injury and Injury Tolerances of the Thorax-Shoulder Complex*, S. Backaitis, Editor. 1994, SAE, Inc.: Warrendale, PA. p. 949-972.
15. Kallieris, D., R. Mattern, G. Schmidt, and R.H. Eppinger. *Quantification of side impact responses and injuries*. in *Stapp Car Crash Conf*. 1981. San Francisco, CA.
16. Maltese, M.R., R.H. Eppinger, H.H. Rhule, B.R. Donnelly, F.A. Pintar, et al., *Response corridors of human surrogates in lateral impacts*. *Stapp Car Crash J*, 2002. **46**: p. 321-51.

17. Pintar, F.A., N. Yoganandan, M.H. Hines, M.R. Maltese, J. McFadden, et al. *Chestband analysis of human tolerance to side impact*. in *Stapp Car Crash Conf.* 1997. Lake Buena Vista, FL.
18. Pintar, F.A., D.J. Maiman, and N. Yoganandan. *Occupant dynamics and injuries in narrow-object side impact*. in *Experimental Safety of Vehicles*. 2007. Lyon, France.
19. Hallman, J.J., N. Yoganandan, and F.A. Pintar, *Biomechanical and injury response to posterolateral loading from torso side airbags*. *Stapp Car Crash Journal*, 2010: p. 227-257.
20. Hallman, J.J., N. Yoganandan, and F.A. Pintar, *Thoracic injury metrics with side air bag: stationary and dynamic occupants*. *Traffic Inj Prev*, 2010. **11**(4): p. 433-42.
21. AIS, *The Abbreviated Injury Scale*, AAAM, Editor. 1990, American Association for Automotive Medicine: Arlington Heights, IL. p. 74.
22. Rhule, H.H., M.R. Maltese, B.R. Donnelly, R.H. Eppinger, J.K. Brunner, et al., *Development of a new biofidelity ranking system for anthropomorphic test devices*. *Stapp Car Crash J*, 2002. **46**: p. 477-512.
23. Yoganandan, N., F.A. Pintar, and M.R. Maltese, *Biomechanics of abdominal injuries*. *Crit Rev Biomed Eng*, 2001. **29**(2): p. 173-246.